

Determining g_A/g_V with High Resolution Spectral Measurements Using an LiInSe_2 Bolometer

A.F. Leder,^{1,2,*} D. Mayer,^{1,†} J. L. Ouellet,¹ F. A. Danevich,³ L. Dumoulin,⁴

A. Giuliani,⁴ J. Kostensalo,⁵ J. Kotila,^{6,7,8} P. de Marcillac,⁴ C. Nones,⁹ V. Novati,⁴

E. Olivieri,⁴ D. Poda,⁴ J. Suhonen,⁶ V.I. Tretyak,³ L. Winslow,^{1,‡} and A. Zolotarova⁹

¹*Massachusetts Institute of Technology, 77 Massachusetts Ave. Cambridge, MA 02139, USA*

²*Department of Nuclear Engineering, University of California - Berkeley, 2521 Hearst Ave, Berkeley, CA 94709, USA*

³*Institute for Nuclear Research of NASU, Kyiv 03028, Ukraine*

⁴*Université Paris-Saclay, CNRS/IN2P3, IJCLab, 91405 Orsay, France*

⁵*Natural Resources Institute Finland, Yliopistokatu 6B, FI-80100 Joensuu, Finland*

⁶*Department of Physics, University of Jyväskylä, P.O. Box 35, FI-40014 Jyväskylä, Finland*

⁷*Finnish Institute for Educational Research, University of Jyväskylä, P.O. Box 35, FI-40014 Jyväskylä, Finland*

⁸*Center for Theoretical Physics, Sloane Physics Laboratory Yale University, New Haven, Connecticut 06520-8120, USA*

⁹*Commissariat à l'Énergie Atomique (CEA)- Saclay, 91191 Gif-sur-Yvette, France*

(Dated: June 22, 2022)

Neutrinoless Double-Beta decay ($0\nu\beta\beta$) processes sample a wide range of intermediate forbidden nuclear transitions, which may be impacted by quenching of the axial vector coupling constant (g_A/g_V), the uncertainty of which plays a pivotal role in determining the sensitivity reach of $0\nu\beta\beta$ experiments. In this Letter, we present measurements performed on a high-resolution LiInSe_2 bolometer in a “source=detector” configuration to measure the spectral shape of the 4-fold forbidden β -decay of ^{115}In . The value of g_A/g_V is determined by comparing the spectral shape of theoretical predictions to the experimental β spectrum taking into account various simulated background components as well as a variety of detector effects. We find evidence of quenching of g_A/g_V at $> 5\sigma$ with a model-dependent quenching factor of 0.655 ± 0.002 as compared to the free-nucleon value for the Interacting Shell Model. We also measured the ^{115}In half-life to be $[5.18 \pm 0.06(\text{stat.})_{-0.015}^{+0.005}(\text{sys.})] \times 10^{14}$ yr within the Interacting Shell Model framework. This work demonstrates the power of the bolometric technique to perform precision nuclear physics single- β decay measurements, which can help reduce the uncertainties in the calculation of $0\nu\beta\beta$ nuclear matrix elements.

INTRODUCTION

From the first observation of single β -decay [1] that led W. Pauli to propose the neutrino [2] and the subsequent efforts to develop a theory of β -decay by E. Fermi [3] to C.S. Wu’s ground-breaking work to determine the vector and axial vector form of the weak interaction [4], the study of β -decay has been used to elucidate the hidden world of nuclear and particle physics. Modern efforts continue this legacy, using nuclear β -decay to investigate the properties of neutrino mass including its absolute scale through endpoint measurements [5–7], and possible Majorana origin through searches for Neutrinoless Double-Beta decay ($0\nu\beta\beta$) [8–16].

In recent years, cryogenic bolometers have established themselves as a powerful technology in rare event searches for $0\nu\beta\beta$ [9, 11–16], direct Dark Matter detection [17–19], and more [20–24]. Such detectors operate at milli-kelvin temperatures and measure energy deposition events by converting phonons into a temperature increase within a sensitive thermistor. Bolometers benefit from excellent energy resolution, high electron containment efficiencies, low energy trigger thresholds, and strong particle-ID capabilities when equipped with a dual heat/light or heat/ionization readout [15, 23, 25]. Additionally, the ability to operate nearly any crystalline ma-

terial as a bolometer provides practical means to study a very wide range of long-lived nuclear processes for which sufficient quantities of isotope may be procured and grown into crystalline form.

As pointed out by [26], theoretical calculations of the nuclear physics contributions to the $0\nu\beta\beta$ half-life have often assumed an axial-to-vector coupling ratio equal to that of the free neutron, $g_A/g_V = 1.276$ [27, 28], though it is common to use a quenched value to obtain agreement with observed single- β transition rates [29–32]. The exact impact on $0\nu\beta\beta$ will depend on the underlying physics of axial quenching [33]; recently Ref. [34] provided evidence that the inclusion of two-nucleon currents and additional correlations may provide an explanation within light ($A \leq 14$) nuclei and certain super-allowed heavy nuclei β -decay transitions. Axial quenching creates a significant uncertainty in the interpretation of any $0\nu\beta\beta$ search when converting isotope-specific half-lives back to the underlying physics of interest [35], on top of the existing spread in the value of calculated Nuclear Matrix Elements (NMEs) for $0\nu\beta\beta$ isotopes [36].

As was proposed in [37], the *shape* of highly-forbidden β -decay spectra can be very sensitive to g_A/g_V , and studying such decays of nuclei with mass around $A \sim 100$ could shed light on axial quenching in a similar nuclear environment as those found in $0\nu\beta\beta$ decays. This anal-

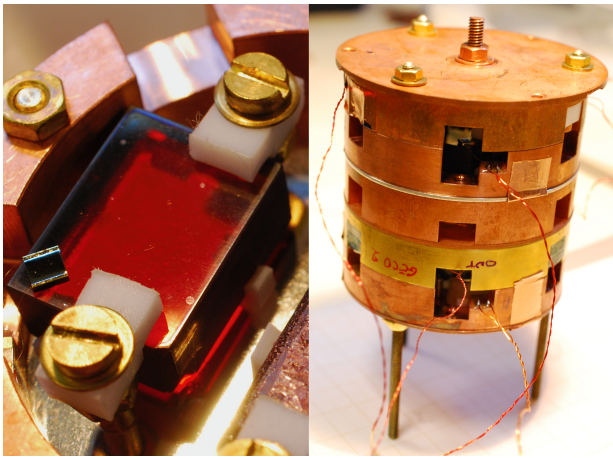


FIG. 1. (Left) Photo of the LiInSe₂ bolometer with an NTD thermistor attached to the crystal. (Right) The combined detector setup in a tower configuration with two pairs of bolometers stacked in two stages. The light detector is placed above each "stage" of the tower for maximum photon absorption

ysis technique could also have applications in explaining reactor flux anomalies through examination of 1st-order forbidden β -decay transitions [38]. This spectral shape technique was used for the first time in [39], where the experimental data from a CdWO₄ scintillation detector [40] were compared to theoretical spectra in order to extract a value for g_A in the range of 0.90–0.93. More recently, COBRA has applied this spectral shape approach to their data of CdZnTe detectors in order to obtain a range for g_A between 0.92 and 0.96 depending on the theoretical models used [41]. In this Letter, we make a precision β -decay spectral shape measurement using a high-resolution "source=detector" bolometer. In particular, we study the 4-fold forbidden β -decay of $^{115}\text{In} \rightarrow ^{115}\text{Sn}$ with $Q_\beta = 497.489$ keV [42] with the most recent previously measured half-life of $(4.41 \pm 0.25) \times 10^{14}$ years [43]. This decay occurs in a mass range relevant to $0\nu\beta\beta$ isotopes of interest and provides a benchmark to test whether many-body nuclear calculations are capable of simultaneously explaining the β -decay spectral shape and rate. Recently, interest has been growing to measure this particular ^{115}In decay mode by examining an In₂O₃ bolometer in order to provide a measurement of g_A/g_V [44]. Here we use a LiInSe₂ crystal with a natural abundance of ^{115}In (95.72 % [45]), to evaluate g_A/g_V for leading nuclear models, and make the most precise measurement of the ^{115}In half-life to date.

METHODS

The LiInSe₂ crystal was grown by RMD Inc. [46] using the vertical Bridgman process [47, 48]. The crystal was enriched in ^6Li to 95% for potential use as a neutron

TABLE I. Experimental parameters of the LiInSe₂ crystal during the October–November 2017 data runs.

Detector Parameter	LiInSe ₂ Crystal
Crystal Dimensions	$1.3 \times 1.6 \times 0.7$ cm
Total Crystal Mass	10.3 grams
Effective ^{115}In Mass	4.1 grams
Noise Level	1.1 keV (1σ)
Avg. Energy Resolution	2.4 keV (1σ)
100 % Trigger Threshold	20.0 keV
Analysis Threshold	160 keV
Containment Eff.	96.6% @ 497 keV
Data Selection Cut Eff.	47.6(2)% (160 – 500 keV)
Livetime Fraction	52.54(8)%
Total Exposure	39.7 g-days

detector [49, 50], however, that analysis is beyond the scope of this work and does not affect the β -decay analysis. The LiInSe₂ crystal was instrumented with a Neutron Transmutation Doped (NTD) thermistor [51], and installed inside a cryostat at IJCLab (ex. CSNSM) in Orsay, France [52], see Fig. 1. The LiInSe₂ scintillation signal was monitored by a separate Neganov-Trofimov-Luke Ge light detector (LD) [53], which allowed us to perform particle identification and pile-up rejection. 42.2 g-days of data was collected over two weeks, with the pertinent measured/derived experimental parameters summarized in Table I.

The data was processed using the APOLLO/DIANA software developed by the CUORE [54]/CUPID-0 [55]/CUORICINO [56] collaborations. Events are triggered with the Optimum Trigger (OT) [57] and processed following a procedure similar to [12, 54]. The trigger threshold was determined by injecting a series of low energy pulses through the attached Joule heater [58], achieving $\sim 100\%$ trigger efficiency above 20 keV. The LiInSe₂ detector is calibrated with a set of dedicated runs with a ^{133}Ba source using the four most prominent γ peaks in the energy range 250–400 keV.

The internal ^{115}In decay on its own results in an expected event rate of ≈ 1.2 Hz in the 10.3 gram LiInSe₂ detector, which means that internal event pile-up is expected to be a significant background. The recovery time after an event is ~ 200 ms, and the event window around each event includes 100 ms before the trigger and 500 ms after. Together, these lead to a significant paralyzable deadtime. The faster response time of the LD allows us to efficiently tag and remove these pile-up events that might otherwise slip through the LiInSe₂ data quality cuts (see Fig. 2), along with tagging α events through particle-identification via event-by-event light-yield cuts.

In order to filter out spurious events from ^{115}In β^- events, a series of loose pulse shape cuts were employed to filter out electrical glitch and badly reconstructed events. Then a rise time pulse quality cut (see Fig. 2) was defined by a 3σ cut band determined by fitting the resulting

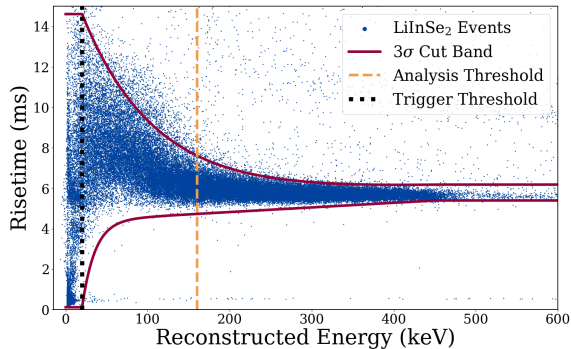


FIG. 2. LiInSe₂ detector events with 3σ cut bands, analysis and trigger thresholds superimposed. The corresponding rise times were collected in 10 keV energy bins running between 20–450 keV and then each bin of rise times were individually fit to a Gaussian. The cut band was then defined by interpolating between the individual 3σ profiles cuts as a function of energy. Outside of the 20–450 keV energy range, the cut values were kept constant due to large uncertainties in the profile fit parameters as a result of non-Gaussian parameter distributions or low statistics at the low/high energy ranges respectively.

pulse shape variable profiles across each energy bin. We also employ a coincidence cut that enforces a single-event criterion. We require that an event is included in the final spectrum if it appears on both the LiInSe₂ and the LD detectors within 20 ms and no other events are recorded on the LiInSe₂ detector within a broader 600 ms window. Over the region of 160–500 keV, we find a cut efficiency of $(47.6 \pm 0.2)\%$, dominated by the LD single-event criterion. The 160 keV threshold was selected as the lowest energy where multiple event pile up was well handled by the autoconvolution background component. The resulting events that pass all the above cuts are then compiled into the input LiInSe₂ spectrum as shown in Fig. 3.

To extract g_A/g_V from the measured LiInSe₂ spectrum, we follow a procedure similar to [59–62] and decompose it into various components: a model-dependent signal component from the β -decay of ¹¹⁵In which will depend on g_A/g_V , an untagged pile-up component, and other radioactive background contributions. The fit is implemented using the Bayesian Analysis Toolkit package [63], which implements a Markov Chain Monte-Carlo (MCMC) to sample the full joint posterior. We perform this decomposition on the spectrum in Fig. 3, which has a binning of 5/30 keV below/above 530 keV respectively up until the analysis cut-off at 1520 keV. This binning scheme allows for the fitting of as many broad spectral/peak features as possible present in the experimental data while maintaining the highest possible statistics per bin in the region beyond 530 keV. Despite the low trigger threshold of the LiInSe₂ crystal, we implement an analysis threshold of 160 keV to avoid low-energy pile-

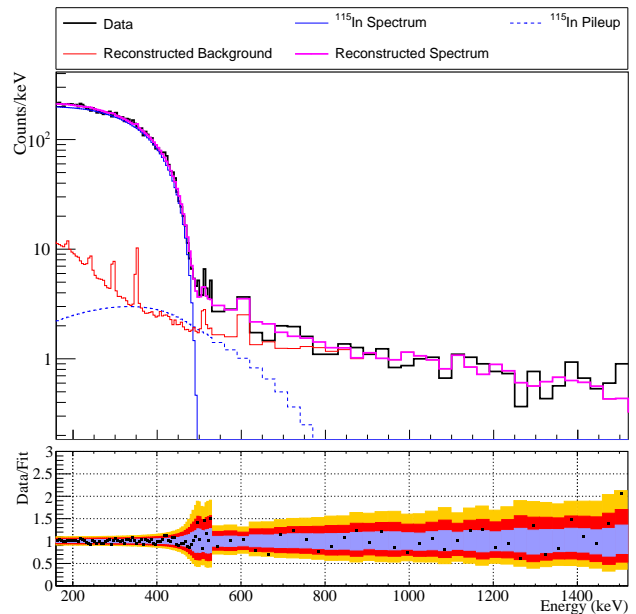


FIG. 3. Spectral fit to the collected LiInSe₂ spectrum over the region 160–1520 keV. Component normalizations and the ¹¹⁵In spectral shape correspond to the best-fit values for the Interacting Shell Model (ISM) exhibiting a χ^2 value of 160 with 101 degrees of freedom. Fits to the Microscopic Quasi-particle-Phonon Model (MQPM) and Interacting Boson Model (IBM) result in similar reconstructions. The bottom panel displays Data/Fit ratios for the reconstruction, along with 1σ (purple), 2σ (red) and 3σ (yellow) fit credibility regions. The spectrum is binned by 5 keV up until 530 keV and by 30 keV above 530 keV in order to maintain reasonable statistics per bin above the ¹¹⁵In endpoint.

up events which are difficult to separate in time and can distort the spectrum.

To implement the MCMC, we define our binned likelihood as:

$$\mathcal{L} = \prod_i \text{Pois} \left(k_i; \sum_j a_j \lambda_{ij} \right), \quad (1)$$

enumerating bins by i and fitted components by j . Here, k_i is the number of observed counts within a given bin, λ_{ij} is the normalized density of the j^{th} component within the i^{th} bin, and a_j are the fitted normalizations for the different components. The densities λ corresponding to ¹¹⁵In are g_A/g_V -dependent.

A numerical calculations for the structure of ¹¹⁵In are performed using ISM [64–66], IBM [67] and MQPM [68]. The resulting β -decay spectrum is generated as a function of energy for each of these structural models taking g_A/g_V as an input. We generate a library of 200 discrete β -decay spectra for g_A/g_V uniformly spaced across the range $0.6 < g_A/g_V < 1.3$ and then perform an interpolation for the spectral shape for g_A/g_V values not in our library. Each ¹¹⁵In spectrum is then convolved with an

energy-dependent detector response function to account for energy losses as well as shifts in the spectral shape from β -particles that escape the absorber. This is calculated through a Geant4 simulation [69] that only simulates the LiInSe₂ crystal and the copper plate it rests on. These simulations find that 96.6% of electrons at the β -decay endpoint will be fully contained within the detector, which represents the minimum containment efficiency over the ¹¹⁵In spectrum. Background component spectra are obtained by simulating in Geant4 various possible radiogenic contaminations including from daughter nuclei on various detector/cryostat components, for example the copper cryostat cold plates and lead shielding surrounding the detector. In total, we simulated the γ/β spectra stemming from ²³⁸U/²³²Th decay chains as well as ⁶⁰Co, and ⁴⁰K decays present uniformly throughout the LiInSe₂ detector, to simulate possible contamination of the various cryostat components particularly the copper plate near the detector, and from external environmental sources. In addition, we simulated a separate background contribution coming solely from possible surface contaminations of the LiInSe₂ crystal. All these input spectra components were then convolved with the detectors' measured energy resolution and binned into the same binning scheme as the data before their use as a potential component of the MCMC fit. The inclusion of a pile-up component (the autoconvolution of the ¹¹⁵In β -spectrum) was designed to account for the inability to separate events which occur too closely in time and could then be mis-reconstructed as a single higher energy event.

The final MCMC fit only included the four most-dominant background components: 1/2) internal crystal contamination stemming from the ²³⁸U decay chains and ⁶⁰Co decays, 3) ²³²Th decay chain events on the copper plate underneath the LiInSe₂ crystal, and 4) ²³²Th decay chain events from external sources mostly in the form of γ s. Contamination from α surface backgrounds can be ignored, thanks to the strong pulse shape and coincidence cuts that were applied to the collected data, resulting in predominantly bulk γ backgrounds. All other simulated background components were found to have only a negligible effect on the final fit parameters. This results in a satisfactory description of background features in the collected spectrum without introducing degeneracies in the fit from additional components which may not be differentiated with available data. We perform a separate fit for each nuclear model tested, and apply uniform priors to the normalizations of each fitted component within the regions of g_A/g_V discussed below.

DISCUSSION

For all three nuclear models examined, the likelihood function within the fit is bi-modal with respect to g_A/g_V , exhibiting a local minimum both at low- g_A/g_V values

below 0.95, and at high- g_A/g_V values above 1.05. Fits arising from the high- g_A/g_V minimum result in a poor match to the observed spectral shape, with decreases in log-likelihood as compared to the low- g_A/g_V minimum of at least 65 (IBM), 90 (MQPM) and 118 (ISM). Despite resulting in an overall worse fit, the high- g_A/g_V fit minima are still sufficiently favored that without a restricted prior, the MCMC chain will take an unreasonably long time to achieve convergence. In order to ensure a good convergence of the MCMC chain about the global minimum while avoiding numerical instabilities, we restrict ourselves to a uniform prior on $g_A/g_V \in [0.6, 1.0]$.

We extract the best-fit values from the maximum a posteriori point (which we will refer to as the “best-fit” values), along with Bayesian Credibility Regions (BCRs) for parameters of interest pertaining to the ¹¹⁵In decay rate and value of g_A/g_V . We marginalize over all background component normalizations as nuisance parameters; all three fits result in compatible contributions from each of the included background components. The best-fit values for g_A/g_V along with the central 1σ BCRs arising from the fits are summarized in Table II. Unsurprisingly, the various nuclear calculations prefer different values of g_A/g_V , however all models strongly reject the free-nucleon value of $g_A/g_V = 1.276$ at $> 5\sigma$ as determined by the $\Delta \log \mathcal{L}$ between the best-fit values and the free-nucleon value, assuming Wilk's theorem [70].

TABLE II. Fit results for each of the three nuclear models considered. For the parameters of interest of g_A/g_V and $T_{1/2}$ for ¹¹⁵In, we quote the best fit value with uncertainty given by the width of the central 68% Bayesian credibility interval, along with the reduced- χ^2 value for the best-fit reconstruction.

Model	g_A/g_V	$T_{1/2}$ (10^{14} yr)	Reduced χ^2
ISM	0.830 ± 0.002	5.177 ± 0.060	1.58
IBM	0.845 ± 0.006	5.031 ± 0.065	1.50
MQPM	0.936 ± 0.003	5.222 ± 0.061	1.60
Pfeiffer et al. [43]		4.41 ± 0.25	
Watt and Glover [71]		5.1 ± 0.4	
Beard and Kelly [72]		6.9 ± 1.5	

Additionally, using the normalization of the ¹¹⁵In component, we can extract the value of the half-life $T_{1/2}({}^{115}\text{In}) = [5.18 \pm 0.06(\text{stat.})_{-0.015}^{+0.005}(\text{sys.})] \times 10^{14}$ years. Here we quote the best-fit value arising from the ISM model fit, with statistical uncertainty determined by the width of the 1σ central BCR with negligible contributions from uncertainties in the cut and live-time efficiencies which are propagated on top of the fitted ¹¹⁵In normalization. We choose to quote the spread in half-life with respect to the IBM and MQPM best-fit values (shown in Table II) as a systematic uncertainty. This is slower by 3σ with respect to the measurement within [43], but falls within 2σ of the older, less precise measurements [71, 72]. Figure 4b) displays the joint 2-dimensional

Bayesian credibility regions for g_A/g_V and $T_{1/2}$ for each fitted nuclear model, along with the best-fit points.

Each of the nuclear models calculations discussed in this letter are able to simultaneously calculate the $T_{1/2}$ as a function of g_A/g_V values [73] as shown by the dash-dotted lines in Figure 4. In our analysis, our best fit values for the half-life given by each model overestimates the half-lives by factors of 1.2 (IBM), 2.2 (MQPM), and 2.0 (ISM) compared to [43], and simultaneously does not fall upon one of the theory curves. This suggests that quenching-dependent calculations that we used are not yet able to simultaneously match the spectral shape and decay rate in ^{115}In . It is worth noting that the half-life in [43] is similarly incapable of simultaneously matching the spectral shape and decay rate.

Previous work with COBRA ^{113}Cd data has shown that the tension between the independently measured half-life and the quenched g_A/g_V values extracted from the spectral shape analysis can be relaxed via the introduction of a small relativistic nuclear matrix element correction that affects the spectral shape due to the enforcement of the conserved vector current assumption [74]. Additionally due to the closeness of our results with the measurements presented in [71, 72], we do not present any conclusion regarding the accuracy of any single nuclear model presented here. This letter seeks to showcase the ability of this technique to simultaneously provide two additional experimental cross checks to any nuclear calculation model, namely spectral shape and half-life, on any provided nuclear model able to address highly forbidden nuclear β -decays.

CONCLUSION

From these data, it is clear that the value of g_A/g_V that governs this highly forbidden decay process is quenched by approximately 0.65–0.75 compared to the decay of the free neutron. Interestingly, for each of the three nuclear models examined there is strong disagreement between the measured half-life from [43] and the predicted half-life value for the favored value of g_A/g_V calculated from spectral shape analysis. This tension could point to possible issues with regards to the many-body approaches and Hamiltonians used in the various calculation frameworks. At the same time, our better agreement with the older measurements of [71, 72] may point to additional systematics effects that could play a vital role in the determination of any half-life measurement/calculation.

This measurement shows the utility of cryogenic bolometers for precision studies across multiple energy bins to test various spectral shapes that stem from rare/forbidden nuclear processes. Further developments in cryogenic detectors which exhibit faster timing resolution, such as those using TESs for heat and/or light readout, would provide better separation of low-energy

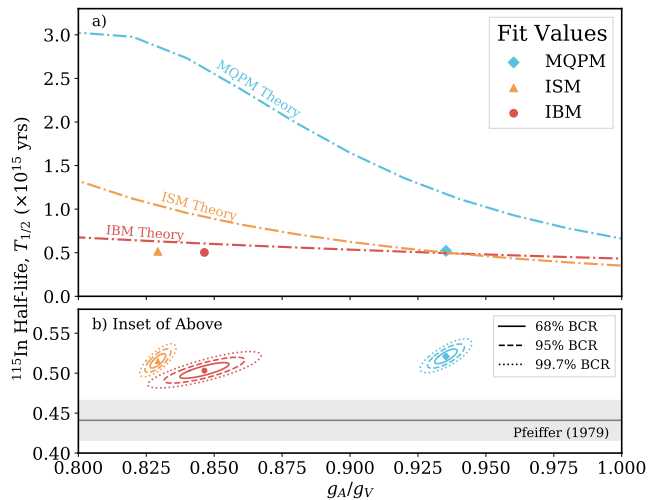


FIG. 4. Top: Half-lives versus g_A/g_V theory curves (dash-dot lines), assuming a conserved vector current [75], for ^{115}In as well as the best fit half-lives and g_A/g_V values (markers) resulting from the spectral-shape fits for the IBM (red), ISM (yellow), and MQPM (cyan) models considered in this Letter. Bottom: Inset of above, focused around the experimentally determined half-life values for ^{115}In . Contours about the best fit values represent the joint two-dimensional Bayesian credibility regions produced from the fit posteriors and only include statistical uncertainties. The previous half-life measurement from [43] is shown in gray with 1σ uncertainty (other measurements omitted for clarity).

pile-up events and could offer even better energy resolutions than the NTDs used in this experiment [25, 76]. Coupled with further improvements in the theory calculations of the nuclear matrix elements [77, 78], this would allow for future studies of ^{115}In and other candidate isotopes for such as ^{113}Cd [74] (for an expanded list see [79]) further increasing the sensitivity to g_A/g_V and opening the door to reducing this source of uncertainty on the nuclear matrix elements utilized by $0\nu\beta\beta$ experiments in their current and projected sensitivity limits.

The dilution refrigerator used for the tests and installed at IJCLab (Orsay, France) was donated by the Dipartimento di Scienza e Alta Tecnologia of the Insubria University (Como, Italy). This work makes use of the DIANA data analysis and APOLLO data acquisition software which has been developed by the CUORICINO, CUORE, LUCIFER, CUPID-Mo and CUPID-0 collaborations. A.F.L. also acknowledges the support of the California Alliance Fellowship. J.K. would like to acknowledge funding from Academy of Finland Grant Nos. 314733 and 345869. This work has also been partially supported by the Academy of Finland under the Academy Project No. 318043. F.A.D. and V.I.T. were supported in part by the National Research Foundation of Ukraine Grant No. 2020.02/0011 and would like to acknowledge the heroic efforts of the Armed Forces of Ukraine.

- * aleder@berkeley.edu
† dmayer@mit.edu
‡ lwinslow@mit.edu
- [1] J Chadwick, “Intensitätsverteilung im magnetischen spektrum der beta-strahlen von radium B+C,” *Verhandlungen der deutschen Physikalischen Gesellschaft* **16**, 383 (1914).
 - [2] Wolfgang Pauli, “Pauli letter collection: letter to Lise Meitner,” (1930).
 - [3] E Fermi, “Versuch einer Theorie der β -Strahlen.” *Zeitschrift für Physik* **88**, 161–177 (1934).
 - [4] C. S. Wu, E. Ambler, R. W. Hayward, D. D. Hoppes, and R. P. Hudson, “Experimental test of parity conservation in beta decay,” *Phys. Rev.* **105**, 1413–1415 (1957).
 - [5] M. Aker, K. Altenmuller, M. Arenz, M. Babutzka, J. Barret, S. Bauer, *et al.*, “Improved Upper Limit on the Neutrino Mass from a Direct Kinematic Method by KATRIN,” *Phys. Rev. Lett.* **123**, 221802 (2019).
 - [6] M. Aker, K. Altenmuller, A. Beglarian, J. Behrens, A. Berlev, U. Besserer, *et al.*, “Analysis methods for the first KATRIN neutrino-mass measurement,” *Phys. Rev. D* **104**, 012005 (2021).
 - [7] M. Aker, A. Beglarian, J. Behrens, A. Berlev, U. Besserer, B. Bieringer, *et al.*, “Direct neutrino-mass measurement with sub-electronvolt sensitivity,” *Nature Physics* **18**, 160–166 (2022).
 - [8] A. Gando, Y. Gando, T. Hachiya, A. Hayashi, S. Hayashida, H. Ikeda, *et al.*, “Search for Majorana Neutrinos Near the Inverted Mass Hierarchy Region with KamLAND-Zen,” *Phys. Rev. Lett.* **117**, 082503 (2016).
 - [9] S.I. Alvis, I.J. Arnquist, F.T. Avignone III, A.S. Barabash, C. J. Barton, V. Basu, *et al.*, “Search for neutrinoless double- β decay in ^{76}Ge with 26 kg yr of exposure from the Majorana Demonstrator Search for Neutrinoless Double- β Decay,” *Phys. Rev. C* **100**, 025501 (2019).
 - [10] G. Anton, I. Badhrees, P. S. Barbeau, D. Beck, V. Belov, T. Bhatta, *et al.*, “Search for Neutrinoless Double- β Decay with the Complete EXO-200 Dataset,” *Phys. Rev. Lett.* **123**, 161802 (2019).
 - [11] M. Agostini, G.R. Araujo, A. M. Bakalyarov, M. Balata, I. Barabanov, L. Baudis, *et al.*, “Final Results of GERDA on the Search for Neutrinoless Double- β Decay,” *Phys. Rev. Lett.* **125**, 252502 (2020).
 - [12] D. Q. Adams, C. Alduino, K. Alfonso, F.T. Avignone III, O. Azzolini, G. Bari, *et al.*, “Improved Limit on Neutrinoless Double-Beta Decay in ^{130}Te with CUORE,” *Phys. Rev. Lett.* **124**, 122501 (2020).
 - [13] D. Q. Adams, C. Alduino, K. Alfonso, F.T. Avignone III, O. Azzolini, G. Bari, *et al.*, “Search for Majorana neutrinos exploiting millikelvin cryogenics with CUORE,” *Nature* **604**, 53–58 (2022).
 - [14] E. Armengaud, C. Augier, A. S. Barabash, F. Bellini, G. Benato, A. Benoit, *et al.*, “New Limit for Neutrinoless Double-Beta Decay of ^{100}Mo from the CUPID-Mo Experiment,” *Phys. Rev. Lett.* **126**, 181802 (2021).
 - [15] O. Azzolini, J.W. Beeman, F. Bellini, M. Beretta, M. Bissoloni, C. Brofferio, *et al.*, “Final Result of CUPID-0 Phase-I in the Search for the ^{82}Se Neutrinoless Double- β Decay,” *Phys. Rev. Lett.* **123**, 032501 (2019).
 - [16] V. Alenkov, H. W. Bae, J. Beyer, R.S. Boiko, K. Boonin, O. Buzanov, *et al.*, “First results from the AMORE-Pilot neutrinoless double beta decay experiment,” *Eur. Phys. J. C* **79**, 791 (2019).
 - [17] A. H. Abdelhameed, G. Angloher, P. Bauer, A. Bento, E. Bertoldo, C. Bucci, *et al.*, “First results from the CRESST-III low-mass dark matter program,” *Phys. Rev. D* **100**, 102002 (2019).
 - [18] I. Alkhatib, D.W.P. Amaral, T. Aralis, T. Aramaki, I.J. Arnquist, I. Atae Langroudy, *et al.*, “Light Dark Matter Search with a High-Resolution Athermal Phonon Detector Operated above Ground,” *Phys. Rev. Lett.* **127**, 061801 (2021).
 - [19] R. Agnese, T. Aralis, T. Aramaki, I.J. Arnquist, E. Azadbakht, W. Baker, *et al.*, “Search for low-mass dark matter with CDMSlite using a profile likelihood fit,” *Phys. Rev. D* **99**, 062001 (2019).
 - [20] C. Augier, G. Beaulieu, V. Belov, L. Berge, J. Billard, G. Bres, *et al.*, “Ricochet Progress and Status,” (2021), [arXiv:2111.06745](https://arxiv.org/abs/2111.06745).
 - [21] I. Alkhatib, D.W.P. Amaral, T. Aralis, T. Aramaki, I.J. Arnquist, I. Atae Langroudy, *et al.*, “Constraints on Lightly Ionizing Particles from CDMSlite,” *Phys. Rev. Lett.* **127**, 081802 (2021).
 - [22] M. Pyle, E. Figueroa-Feliciano, and B. Sadoulet, “Optimized Designs for Very Low Temperature Massive Calorimeters,” (2015), [arXiv:1503.01200](https://arxiv.org/abs/1503.01200) [astro-ph.IM].
 - [23] Denys Poda, “Scintillation in Low-Temperature Particle Detectors,” *Physics* **3**, 473–535 (2021).
 - [24] P. De Marcillac, N. Coron, G. Dambier, J. Leblanc, and J. Moalic, “Experimental detection of α -particles from the radioactive decay of natural bismuth,” *Nature* **422**, 876–878 (2003).
 - [25] R. Huang, E. Armengaud, C. Augier, A.S. Barabash, F. Bellini, G. Benato, *et al.*, “Pulse shape discrimination in CUPID-Mo using principal component analysis,” *Journal of Instrumentation* **16**, P03032 (2021).
 - [26] J. Barea, J. Kotila, and F. Iachello, “Nuclear matrix elements for double beta decay,” *Phys. Rev. C* **87**, 014315 (2013).
 - [27] D. Mund, B. Markisch, M. Deissenroth, J. Krempel, M. Schumann, H. Abele, *et al.*, “Determination of the weak axial vector coupling $\lambda = \frac{g_A}{g_V}$ from a measurement of the β -asymmetry parameter A in neutron beta decay,” *Phys. Rev. Lett.* **110**, 172502 (2013).
 - [28] B. Markisch, H. Mest, H. Saul, X. Wang, H. Abele, D. Dubbers, *et al.*, “Measurement of the Weak Axial-Vector Coupling Constant in the Decay of Free Neutrons Using a Pulsed Cold Neutron Beam,” *Phys. Rev. Lett.* **122**, 242501 (2019).
 - [29] V. Kumar, P. C. Srivastava, and H. Li, “Nuclear β -decay half-lives for fp and fpg shell nuclei,” *J. Phys. G* **43**, 105104 (2016).
 - [30] W. T. Chou, E. K. Warburton, and B. A. Brown, “Gamow-Teller beta-decay rates for $A < 18$ nuclei,” *Phys. Rev. C* **47**, 163–177 (1993).
 - [31] B. Brown, “Status of the Nuclear Shell Model,” *Annu. Rev. Nucl. Part. Sci.* **38**, 29–66 (1988).
 - [32] G. Martínez-Pinedo, A. Poves, E. Caurier, and A. P. Zuker, “Effective g_A in the pf shell,” *Phys. Rev. C* **53**, R2602—R2605 (1996).
 - [33] J. Suhonen, “Value of the axial-vector coupling strength in β and $\beta\beta$ decays: A review,” *Frontiers in Physics* **5**, 55 (2017).
 - [34] P. Gysbers, G. Hagen, J.D. Holt, G.R. Jansen, T.D. Mor-

- ris, P. Navratil, *et al.*, “Discrepancy between experimental and theoretical β -decay rates resolved from first principles,” *Nature Phys.* **15**, 428–431 (2019).
- [35] M.J. Dolinski, A.W. Poon, and W. Rodejohann, “Neutrinoless Double-Beta Decay: Status and Prospects,” *Annu. Rev. Nucl. Part. Sci.* **69**, 219–251 (2019).
- [36] J. Engel and J. Menéndez, “Status and future of nuclear matrix elements for neutrinoless double-beta decay: A review,” *Rep. Prog. Phys.* **80**, 046301 (2017).
- [37] M. Haaranen, P. C. Srivastava, and J. Suhonen, “Forbidden nonunique beta decays and effective values of weak coupling constants,” *Phys. Rev. C* **93**, 034308 (2016).
- [38] L. Hayen, J. Kostensalo, N. Severijns, and J. Suhonen, “First-forbidden transitions in the reactor anomaly,” *Phys. Rev. C* **100**, 054323 (2019).
- [39] A. Alessandrello, C. Brofferio, D.V. Camin, O. Cremonesi, F.A. Danevich, P. de Marcillac, *et al.*, “Bolometric measurement of the beta spectrum of ^{113}Cd ,” *Nucl. Phys. B (Proc. Suppl.)* **35**, 394–396 (1994).
- [40] P. Belli, R. Bernabei, N. Bukilic, F. Cappella, R. Cerulli, C.J. Dai, *et al.*, “Investigation of β decay of ^{113}Cd ,” *Phys. Rev. C* **76**, 064603 (2007).
- [41] L. Bodenstern-Dresler, Y. Chu, D. Gehre, C. Gossling, A. Heimbald, C. Herrmann, *et al.*, “Quenching of g_A deduced from the β -spectrum shape of ^{113}Cd measured with the COBRA experiment,” *Phys. Lett. B* **800**, 135092 (2020).
- [42] M. Wang, W.J. Huang, F.G. Kondev, G. Audi, and S. Naimi, “The AME 2020 atomic mass evaluation (II). Tables, graphs and references,” *Chinese Phys. C* **45**, 030003 (2021).
- [43] L. Pfeiffer, A.P. Mills, E.A. Chandross, and T. Kovacs, “Beta spectrum of ^{115}In ,” *Phys. Rev. C* **19**, 1035–1041 (1979).
- [44] E. Celi, Z. Galazka, M. Laubenstein, S. Nagorny, L. Pagnanini, S. Pirro, *et al.*, “Development of a cryogenic In_2O_3 calorimeter to measure the spectral shape of ^{115}In β -decay,” *Nucl. Instrum. Methods Phys. Res. A* **1033**, 166682 (2022).
- [45] J. Meija, T. Coplen, M. Berglund, W. Brand, P. De Bièvre, M. Groning, *et al.*, “Isotopic compositions of the elements 2013 (IUPAC Technical Report),” *Pure and Applied Chemistry* **88**, 293–306 (2016).
- [46] 44 Hunt Street, Watertown, MA 02472, email: info@rmdinc.com, website: rmdinc.com.
- [47] L. Isaenko, I. Vasilyeva, A. Merkulov, A. Yelisseyev, and S. Lobanov, “Growth of new nonlinear crystals LiMX_2 (M=Al, In, Ga; X=S, Se, Te) for the mid-IR optics,” *J. Cryst. Growth* **275**, 217–223 (2005).
- [48] J. Tower, L. Winslow, A. Churilov, Y. Ogorodnik, H. Hong, J. Glodo, *et al.*, “New scintillating bolometer crystals for rare particle detection,” *Nucl. Instrum. Methods Phys. Res. A* **954**, 162300 (2020).
- [49] Z. W. Bell, A. Burger, L. Matei, M. Groza, A. Stowe, J. Tower, *et al.*, “Neutron detection with LiInSe_2 ,” in *Hard X-Ray, Gamma-Ray, and Neutron Detector Physics XVII*, Vol. 9593 (SPIE, 2015) pp. 20–32.
- [50] E. Tupitsyn, P. Bhattacharya, and E. Rowe, “Single crystal of LiInSe_2 semiconductor for neutron detector,” *Appl. Phys. Lett.* **101**, 2–5 (2012).
- [51] E.E. Haller, N.P. Palaio, M. Rodder, W.L. Hansen, and E. Kreysa, “NTD Germanium: A Novel Material for Low Temperature Bolometers,” in *Neutron Transmutation Doping of Semiconductor Materials*, edited by R. D. Larrabee (Springer US, 1984) pp. 21–36.
- [52] F. A. Danevich, V.Ya. Degoda, L.L. Dulger, L. Dumoulin, A. Giuliana, P. de Marcillac, *et al.*, “Growth and characterization of a $\text{Li}_2\text{Mg}_2(\text{MoO}_4)_3$ scintillating bolometer,” *Nucl. Instrum. Methods Phys. Res. A* **889**, 89–96 (2018).
- [53] V. Novati, L. Berge, L. Dumoulin, A. Guiliana, M. Mancuso, P. de Marcillac, *et al.*, “Charge-to-heat transducers exploiting the Neganov-Trofimov-Luke effect for light detection in rare-event searches,” *Nucl. Instrum. Methods Phys. Res. A* **940**, 320–327 (2019).
- [54] C. Alduino, K. Alfonso, D. R. Artusa, F.T. Avignone III, O. Azzolini, T.I. Banks, *et al.*, “Analysis techniques for the evaluation of the neutrinoless double- β decay lifetime in ^{130}Te with the CUORE-0 detector,” *Phys. Rev. C* **93**, 045503 (2016).
- [55] O. Azzolini, M. T. Barrera, J.W. Beeman, F. Bellini, M. Beretta, M. Biassoni, *et al.*, “Analysis of cryogenic calorimeters with light and heat read-out for double beta decay searches,” *Eur. Phys. J. C* **78**, 734 (2018).
- [56] E. Andreotti, C. Arnaboldi, F.T. Avignone III, M. Balata, I. Bandac, M. Barucci, *et al.*, “ ^{130}Te neutrinoless double-beta decay with CUORICINO,” *Astroparticle Physics* **34**, 822–831 (2011).
- [57] S. Di Domizio, F. Orio, and M. Vignati, “Lowering the energy threshold of large-mass bolometric detectors,” *Journal of Instrumentation* **6**, P02007 (2011).
- [58] E. Andreotti, C. Brofferio, L. Foggetta, A. Giuliana, B. Margesin, C. Nones, *et al.*, “Production, characterization, and selection of the heating elements for the response stabilization of the CUORE bolometers,” *Nucl. Instrum. Methods Phys. Res. A* **664**, 161–170 (2012).
- [59] D. Q. Adams, C. Alduino, K. Alfonso, F.T. Avignone III, O. Azzolini, G. Bari, *et al.*, “Measurement of the $2\nu\beta\beta$ Decay Half-Life of ^{130}Te with CUORE,” *Phys. Rev. Lett.* **126**, 171801 (2021).
- [60] O. Azzolini, J.W. Beeman, F. Bellini, M. Beretta, M. Biassoni, C. Brofferio, *et al.*, “Evidence of Single State Dominance in the Two-Neutrino Double- β Decay of ^{82}Se with CUPID-0,” *Phys. Rev. Lett.* **123**, 262501 (2019).
- [61] E. Armengaud, C. Augier, A.S. Barabash, F. Bellini, G. Benato, A. Benoit, *et al.*, “Precise measurement of $2\nu\beta\beta$ decay of ^{100}Mo with the CUPID-Mo detection technology,” *Eur. Phys. J. C* **80**, 674 (2020).
- [62] C. Alduino, K. Alfonso, D.R. Artusa, F.T. Avignone III, O. Azzolini, T.I. Banks, *et al.*, “Measurement of the two-neutrino double-beta decay half-life of ^{130}Te with the CUORE-0 experiment,” *Eur. Phys. J. C* **77**, 13 (2017).
- [63] A. Caldwell, D. Kollár, and K. Kröninger, “BAT – The Bayesian analysis toolkit,” *Computer Physics Communications* **180**, 2197–2209 (2009).
- [64] Y. Iwata, N. Shimizu, T. Otsuka, Y. Utsuno, J. Menéndez, M. Honma, *et al.*, “Large-Scale Shell-Model Analysis of the Neutrinoless $\beta\beta$ Decay of ^{48}Ca ,” *Phys. Rev. Lett.* **116**, 112502 (2016).
- [65] J. Menéndez, A. Poves, and E. Caurier, “Disassembling the nuclear matrix elements of the neutrinoless $\beta\beta$ decay,” *Nucl. Phys. A* **818**, 139–151 (2009).
- [66] M. Horoi and A. Neacsu, “Shell model predictions for ^{124}Sn double- β decay,” *Phys. Rev. C* **93**, 024308 (2016).
- [67] J. Barea, J. Kotila, and F. Iachello, “ $0\nu\beta\beta$ and $2\nu\beta\beta$ nuclear matrix elements in the interacting boson model with isospin restoration,” *Phys. Rev. C* **91**, 034304 (2015).
- [68] J. Toivanen and J. Suhonen, “Microscopic quasiparticle-

- phonon description of odd-mass,” *Phys. Rev. C* **57**, 1237–1245 (1998).
- [69] J. Allison, K. Amako, and J. Apostolakis, “Recent developments in GEANT4,” *Nucl. Instrum. Methods Phys. Res. A* **835**, 186–225 (2016).
- [70] S.S. Wilks, “The Large-Sample Distribution of the Likelihood Ratio for Testing Composite Hypotheses,” *The Annals of Mathematical Statistics* **9**, 60–62 (1938).
- [71] D.E. Watt and R.N. Glover, “A search for radioactivity among the naturally occurring isobaric pairs,” *The Philosophical Magazine: A Journal of Theoretical Experimental and Applied Physics* **7**, 105–114 (1962).
- [72] G.B. Beard and W.H. Kelly, “Beta Decay of Naturally Radioactive In^{115} ,” *Phys. Rev.* **122**, 1576–1579 (1961).
- [73] M. Haaranen, J. Kotila, and J. Suhonen, “Spectrum-shape method and the next-to-leading-order terms of the β -decay shape factor,” *Phys. Rev. C* **95**, 024327 (2017).
- [74] J. Kostensalo, J. Suhonen, J. Volkmer, S. Zatschler, and K. Zuber, “Confirmation of g_A quenching using the revised spectrum-shape method for the analysis of the ^{113}Cd β -decay as measured with the COBRA demonstrator,” *Phys. Lett. B* **822**, 136652 (2021).
- [75] R.P. Feynman and M. Gell-Mann, “Theory of the Fermi Interaction,” *Phys. Rev.* **109**, 193–198 (1958).
- [76] A. Armatol, E. Armengaud, W. Armstrong, C. Augier, F.T. Avignone III, O. Azzolini, *et al.*, “Novel technique for the study of pileup events in cryogenic bolometers,” *Phys. Rev. C* **104**, 015501 (2021).
- [77] A. Kumar, P. C. Srivastava, J. Kostensalo, and J. Suhonen, “Second-forbidden nonunique β^- decays of ^{24}Na and ^{36}Cl assessed by the nuclear shell model,” *Phys. Rev. C* **101**, 064304 (2020).
- [78] A. Kumar, P. C. Srivastava, and J. Suhonen, “Second-forbidden nonunique β^- decays of $^{59,60}\text{Fe}$: possible candidates for g_A sensitive electron spectral-shape measurements,” *Eur. Phys. J. A* **57**, 225 (2021).
- [79] H. Ejiri, J. Suhonen, and K. Zuber, “Neutrino–nuclear responses for astro-neutrinos, single beta decays and double beta decays,” *Physics Reports* **797**, 1–102 (2019).